CrossMark

ORIGINAL ARTICLE

A simulator for advanced analysis of a 5-DOF EM tracking systems in use for image-guided surgery

Mengfei Li[1,2] · **Christian Hansen**[2] · **Georg Rose**[1]

Abstract

Purpose To assess the accuracy of medical electromagnetic tracking systems, reference positioning systems are generally required. Errors are unavoidable in such systems, and despite how tiny they may be, prevent the ground truth from being known. In this work, a simulator was developed and used to analyze the theoretical system performances in electromagnetic tracking.

Methods To simulate the entire tracking process, the magnetic dipole model, Faraday's law, and a mathematical optimization algorithm are applied. With the simulator, we optimized the spatial placement of the transmitter coils, analyzed the tracking accuracy by applying stochastic and optimized coil placement. Additionally, the performance of the calibration of transmitter coils' measurement error and Kalman filtering was tested.

Results The results show that, after optimizing the spatial arrangement of the transmitter coils, the tracking accuracy is significantly improved to a much higher level compared with applying statistical arrangement. The measurement errors of the transmitter coils' positions and orientations can be totally rectified by the developed calibration algorithm when no noises are introduced. The Kalman filter reduces the sensor jitter errors caused by noise, which potentially allows the EM tracking system to reach a larger volume of interest.

Conclusions We proposed a simulator for advanced analysis in electromagnetic tracking without hardware requirements. Grounded on this, we performed an optimization of the spatial arrangement of the transmitter coils to improve the tracking accuracy further. The performances of the calibration algorithm and Kalman filtering were also evaluated. The developed simulator can also be applied for other analysis in electromagnetic tracking.

✉ Mengfei Li
  mengfei.li@ovgu.de

1 Chair for Medical Telematics and Medical Technology, Institute of Medical Technology, Otto-von Guericke Universität Magdeburg, Universitätsplatz 2, 39016 Magdeburg, Germany

2 Research Group of Computer-Assisted Surgery, Institute of Simulation and Graphics, Otto-von-Guericke Universität Magdeburg, Universitätsplatz 2, 39016 Magdeburg, Germany

Introduction

Electromagnetic tracking systems (EMTS) have become more widely applied in clinical settings, such as supporting radiation therapy [1], computer tomography and ultrasound-guided interventions [2,3]. EMTS register the position and orientation (pose) of the tracker tool relative to the pre-scanned patient anatomy [4]. The small size magnetic sensor can be mounted into medical instruments such as needles and catheters [5]. The non-line-of-sight operation of EMTS makes it advantageous in particular tracking applications, such as movement of a flexible instrument within the patient's body [6]. To provide adequate tracking information and meet safety requirements, accuracy is one most significant issue for medical EMTS [7]. However, various error sources can negatively influence the tracking accuracy.

The jitter errors of EMTS increase when the working volume becomes larger [8] which limits the volume of interest (VOI) for accurate tracking. Unavoidable metallic objects in the OR, such as surgical instruments proximate to the sensor coil, cause significant errors in estimated sensor pose

[9]. Errors in the measurement of mechanically predefined poses of the transmitter coils also reduce the tracking accuracy [10]. For supporting instrument tracking in IGS, the coordinate system of the EMTS should be registered with the pre-scanned patient anatomy, introducing registration error [11]. The stationary and moving metallic material and electronic devices located in proximity to the sensor coil cause additional tracking error. Moreover, considering the dynamic performance of EMTS, the sensor velocity becomes another source of error. It is difficult to separate all these sources of error in evaluating the tracking accuracy in reality [4]. However, different sources of errors can be easily separated and individually analyzed by using the simulator.

In evaluating the tracking accuracy, groups have proposed different assessment protocols. Reference positioning systems are commonly utilized [8,12–16]. Test phantom-based assessments in evaluating EMTS tracking accuracy are suggested in the literature [8,14,15]. Precisely pre-bored holes in different directions with certain depths provide reference positions where the EM sensor can be manually inserted. More quantitative measurements are not always possible with such phantom-based evaluations. Another simple and low-cost way is to use modular bricks from LEGO (The LEGO Group, Denmark). Different volumetric structure can be freely built for various measurements [16,17]. Significant errors can exist in the manually built LEGO towers. 3D robotic coordinate measuring machines [18] and three-axis robots have high volumetric accuracy. For such evaluations, the sensor coil was fixed on a robot arm and moved in the measurement volume to multiple locations [13]. These robot-based tracking systems normally serve in a large volume, and the arm movement can be freely programmed. However, the metallic structure could negatively influence on the tracker accuracy. Compared to EMTS, which usually require a less than 2 mm positioning error in estimated sensor pose, optical tracking systems (OTS) have a much higher accuracy of than EMTS [18], which can be utilized as reference positioning systems to access the tracker accuracy of EMTS [12]. For the methods introduced above, tracking errors of some magnitude always exist in the reference positioning systems. In this work, an EMTS simulator was developed to provide the exact locations of the sensor as ground truth.

As referred in [4], commercial EMTS have different field generator comprising multiple transmitter coils. However, the spatial arrangement of the transmitter coils is confidential for the manufacturers. EMTS with various shape of field generators have different accuracy [19]. In scientific papers [20,21], the standard coil arrangement was given without being optimized. This work presents the evaluation of tracking accuracy according to different transmitter coil arrangements and the corresponding optimization solutions based on self-developed simulation software for EMTS. The

simulator allows statistical analysis to be performed without difficulties in separating sources of error, difficulties in construction or large time consumption.

Background theory

EM tracking

EMTS have commonly multiple transmitter coils and at least one sensor coil [22]. In this work, we focus on five-degree-of-freedom (5-DOF) EMTS generally applied in assisting IGS. To simulate the generated magnetic field, magnetic dipole approximation is utilized [23], to simplify the computational processes and increase the tracking speed. The calculation of magnetic field flux density is given by (1):

$$\vec{B_i} = \frac{\mu}{4\pi} \left(\frac{\left(3\left(\vec{x_s} - \vec{r_{t,i}}\right) \cdot \left(\vec{m_{t,i}} \cdot \left(\vec{x_s} - \vec{r_{t,i}}\right)\right)\right)}{|\vec{x_s} - \vec{r_{t,i}}|^5} - \frac{\vec{m_{t,i}}}{|\vec{x_s} - \vec{r_{t,i}}|^3} \right) \tag{1}$$

where μ is the coil's magnetic permeability, $\vec{x_s} = \begin{pmatrix} X_s \\ Y_s \\ Z_s \end{pmatrix}$ is the position of the sensor coil and $\vec{r_{t,i}} = \begin{pmatrix} X_{t,i} \\ Y_{t,i} \\ Z_{t,i} \end{pmatrix}$ is the position of the i-th transmitter coil toward X, Y and Z direction in the 3D Cartesian coordinate system of the magnetic field. $\vec{m_{t,i}}$ is the magnetic dipole moment which can be calculated using (2):

$$\vec{m_{t,i}} = \pi \cdot N_{t,i} \cdot I_{t,i} \cdot R_{t,i}^2 \cdot \vec{r_{t,i}} \cdot \begin{pmatrix} \sin \Theta_{t,i} \cos \Phi_{t,i} \\ \sin \Theta_{t,i} \sin \Phi_{t,i} \\ \cos \Theta_{t,i} \end{pmatrix} \tag{2}$$

where $N_{t,i}$ represents the turns of the windings, $I_{t,i}$ is the current flow, $R_{t,i}$ is the radius, and $\Phi_{t,i}$ and $\Theta_{t,i}$ are the yaw and pitch Euler angles of the i-th transmitter coil. Knowing the magnetic field flux density and the parameters of the transmitter and sensor coil, the voltage induced in the sensor coil can be calculated using (3).

$$U_{est,i} = \omega \cdot A_s \cdot N_s \cdot \vec{B_i} \cdot \begin{pmatrix} \sin \Theta_s \cos \Phi s \\ \sin \Theta_s \sin \Phi s \\ \cos \Theta_s \end{pmatrix} \tag{3}$$

where, ω is the angular frequency of the generated AC magnetic field, A_s is the cross-sectional area of the sensor coil, and N_s is the number of the turns of the sensor coil. It should be noted that, generally, the amplitude of the voltage is proportional to the frequency. However, in reality, this
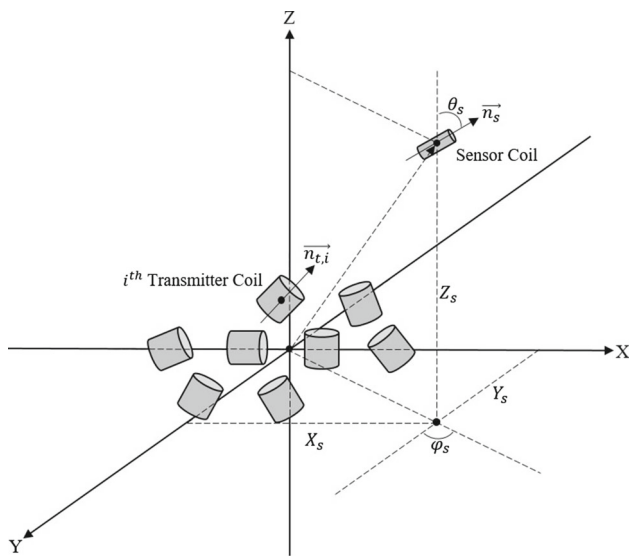
Fig. 1 Estimated 5-DOF sensor pose; X_s, Y_s, Z_s present the estimated sensor location in 3D Cartesian coordinate systems while Φ_s and Θ_s present the yaw and pitch Euler angles

is valid just for a certain frequency bandwidth, defined by the restricted bandwidth of the applied amplifiers and low-pass filters of the circuits. Furthermore, the inductance of the coils also influences the range of the bandwidth, considering the self-resonance. The pitch and yaw angles of the sensor are represented by Φ_s and Θ_s. Optimization algorithms such as Levenberg–Marquardt algorithm [24] can determine the nonlinear parameters of sensor pose. The objective function is presented by (4).

$$F(X_s, Y_s, Z_s, \Phi_s, \Theta_s) = \sum_{i=1}^{k} (U_{\text{mea},i} - U_{\text{est},i})^2 \qquad (4)$$

Here, k represents the number of the transmitter coils, which should be equal or greater than 5 in order to estimate the five variables.

The arrangement of the transmitter coils in Fig. 1 is an example of a typical EMTS. Different coil arrangements have been proposed by research groups [20–22] regarding overall accuracy, minimum space occupied by all coils, and placement on a 2D plane, respectively. In our experiments, we focused on arranging the transmitter coils in one plane within a small box [10].

Calibration of the measurement errors in transmitter coils' poses

Human-eye-based measurement of the transmitter coil positions and orientations is very error-prone, thus strongly degrading the tracking accuracy of EMTS. Bien et al. developed a calibration method to compensate the pose errors

of the transmitter coils using an optimization algorithm as described in [10]. Assuming the deviations of the transmitter coils' poses are $\triangle X_{t,i}$, $\triangle Y_{t,i}$, $\triangle Z_{t,i}$, $\triangle \Phi_{t,i}$ and $\triangle \Theta_{(t,i)}$, the real locations and the orientations of the transmitter coils are given by Eqs. (5) and (6).

$$\overrightarrow{r_{t,i}} = \begin{pmatrix} X_{t,i} + \triangle X_{t,i} \\ Y_{t,i} + \triangle Y_{t,i} \\ Z_{t,i} + \triangle Z_{t,i} \end{pmatrix} \qquad (5)$$

$$\overrightarrow{n_i} = \begin{pmatrix} \sin(\Theta_{t,i} + \triangle \Theta_{t,i}) \cos(\Phi_{t,i} + \triangle \Phi_{t,i}) \\ \sin(\Theta_{t,i} + \triangle \Theta_{t,i}) \sin(\Phi_{t,i} + \triangle \Phi_{t,i}) \\ \cos(\Theta_{t,i} + \triangle \Theta_{t,i}) \end{pmatrix} \qquad (6)$$

Firstly, a certain number of pose measurements of the randomly positioned sensing coil must be performed. For each position, the induced currents in the testing coil by all sending coils were recorded, and the true position was detected by an additional optical tracking system. The optimization procedure was about finding best deviations $\triangle X_{t,i}$, $\triangle Y_{t,i}$, $\triangle Z_{t,i}$, $\triangle \Phi_{t,i}$ and $\triangle \Theta_{t,i}$, which cause identical EMTS' sensor position estimates as given by the optical system.

Kalman filtering

Kalman filter is widely applied in different tracking modalities to improve the accuracy [25,26]. In EM tracking, the noises in the estimated sensor pose are typically assumed as Gaussian noise [4]. In principle, Kalman filter can be applied to reduce the jitter errors. For catheter tracking in medical applications, the constant velocity movement model was proposed [27]. The system state vector is defined as $x_k = \begin{pmatrix} X_s, Y_s, Z_s, \Phi_s, \Theta_s \\ \dot{X}_s, \dot{Y}_s, \dot{Z}_s, \dot{\Phi}_s, \dot{\Theta}_s \end{pmatrix}$ including the sensor poses, linear and angular velocities. In this work, we have implemented the Kalman filter into the simulator and evaluated its performance without considering the localization errors due to the measurement setups.

Method and materials

The simulator

In this work, an EMTS simulator was developed to simulate the entire system flow based on the general AC EM tracking concept [10,20,21]. In practice, to evaluate the tracking accuracy, the reference poses of the sensor coil are provided by another positioning system. The actual sensor positions cannot be guaranteed since the measurement error always exists. This issue can be perfectly solved using the simulator, in which the ground truth of sensor pose can be predefined. Based on the real sensor pose, inversely, the voltage induced
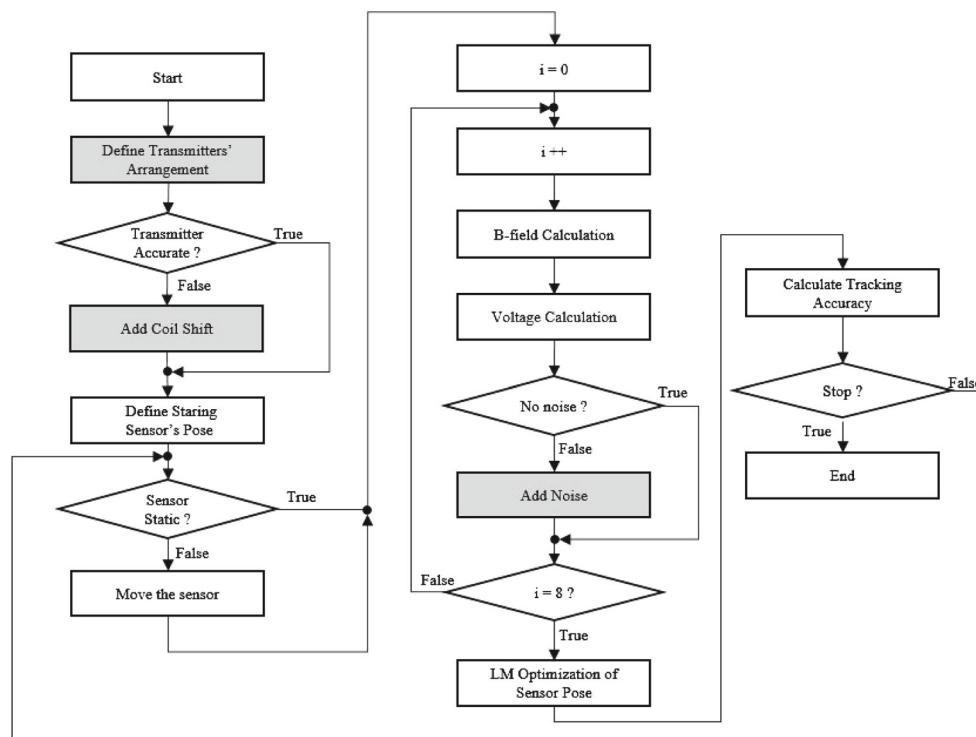
Fig. 2 The flow chart of the developed EMTS simulator

in the sensor coil can be calculated as the "measured" voltages. In reality, noises in voltage measurement and errors in the reference positioning systems always exist, while in the simulator artificial noise signals can be selectively added or wholly excluded. Figure 2 shows the workflow of the developed EMTS simulator.

After the program starts, we firstly defined the poses of the transmitter coils and the starting pose of the sensor coil. Errors in the transmitter coils' poses can be added. The sensor can be fixed at one location or moved following the implemented movement models for statistical analysis. Each transmitter coil is activated sequentially to generate magnetic fields. The voltages induced in each transmitter coil are estimated. Noise signals can be added into the voltages of each channel individually. After acquiring the voltages induced by eight transmitter coils, the sensor's pose was estimated by utilizing the 'fsolve' function in *MATLAB* (Mathworks, USA). The tracking accuracy, influenced by the transmitter coils' arrangement with standard noises in measured voltages, was evaluated.

Accuracy assessment of simulations

In this work, the testing volume was chosen to be $500 \times 500 \times 500$ mm because this it is reported to be a typical volume of interest (VOI) for medical applications. The starting position

of the coil was $\begin{pmatrix} -250\,\text{mm} \\ -250\,\text{mm} \\ 50\,\text{mm} \end{pmatrix}$. Considering the height of the

transmitter coils, the sensor coil was initially moved 50 mm away from the origin in the Z direction. After the measurement began, the sensor coil was moved in the X direction with a step size of 50mm for 11 steps. For each X location the sensor was additionally moved in the Y direction with the same step distance, resulting in 121 positions for one X–Y plane. In the next step, the sensor was moved 100 mm in the Z direction before repeating the scanning within the X–Y plane. In total we analyzed 6 layers, each at 121 locations, resulting in 726 poses of the sensor coil. The starting orientation of

the sensor was selected to be $\begin{pmatrix} -180° \\ -180° \end{pmatrix}$, with the increasing

step for each location being $360° \div 726 = 0.4959°$. After one complete measurement, the position and orientation of

the sensor were increased to $\begin{pmatrix} 250\,\text{mm} \\ 250\,\text{mm} \\ 50\,\text{mm} \end{pmatrix}$ and $\begin{pmatrix} 180° \\ 180° \end{pmatrix}$. The

defined reference positions and orientations of the sensor coil within the simulator are presented by Fig. 3.

A simple noise model, additive Gaussian white noise (AGWN), has been added to the "measured" voltages. For particular systems, different noise levels or noise models can be assumed. In this work, the noise level was selected to be -100 dBW as a standard, for all the scenarios. The sensor pose error calculation is given by (7) and (8):
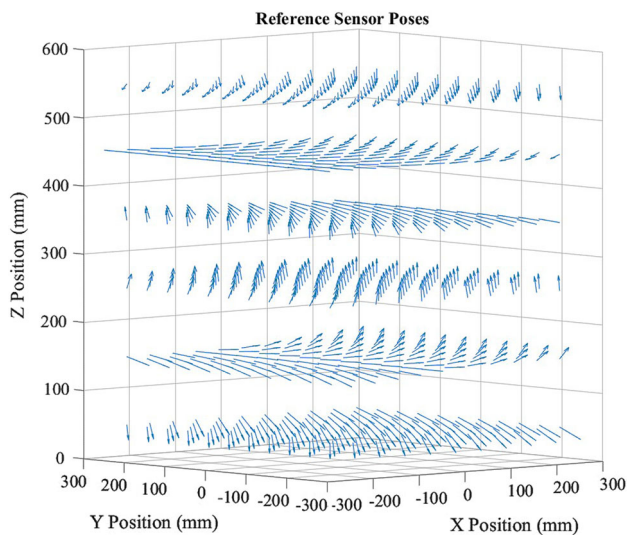
Fig. 3 The reference positions and orientations of the sensor coil defined within the simulator

$$E_{p,j} = \sqrt{(X_{m,j} - X_{r,j})^2 + (Y_{m,j} - Y_{r,j})^2 + (Z_{m,j} - Z_{r,j})^2} \tag{7}$$

$$E_{o,j} = |\Phi_{m,j} - \Phi_{r,j}| + |\Theta_{m,j} - \Theta_{r,j}| \tag{8}$$

where j illustrates the sensor coil placed in j different locations. The sensor reference poses are $X_{r,j}$, $Y_{r,j}$, $Z_{r,j}$ and $\Phi_{r,j}$, $\Theta_{r,j}$ and the calculated sensor poses are $X_{m,j}$, $Y_{m,j}$, $Z_{m,j}$ and $\Phi_{m,j}$, $\Theta_{m,j}$ By using the EMTS simulator, the reference sensor pose is defined directly in the software as ground truth.

Optimizing of the transmitter coils' spatial arrangement

The signal quality, represented by the signal to noise ratio (SNR) of the measured voltages, influences the tracking accuracy [28]. As seen in Eqs. (1–3), the poses of the transmitter coils and the sensor coil affect the amplitude of the voltages induced by the transmitter coils. The aim is to find the maximum of the measured mean voltage U_{mean} for all the testing points by changing the spatial arrangement of the transmitter coils. *MATLAB* "patternsearch" function was selected to realize this optimization process. In this application, the objective function to be optimized is chosen to be the absolute value of the reciprocal of the mean voltage, which is given by Eq. (9):

$$F_1 = \left| \frac{1}{U_{\mathrm{mean}}} \right| \tag{9}$$

Herein, 726 positions of the sensor coil were chosen, and at each position, the sensor coil was vertically faced to the XY, XZ and YZ planes individually. Therefore $726 \times 3 = 2178$ sensor poses were used. The vector coils' arrangement to be optimized is defined as an 8×5 matrix, as Eq. (10) presents:

$$\triangle x = \begin{bmatrix} \triangle X_1 & \triangle Y_1 & \triangle Z_1 & \triangle \Phi_1 & \triangle \Theta_1 \\ \triangle X_2 & \triangle Y_2 & \triangle Z_2 & \triangle \Phi_2 & \triangle \Theta_2 \\ . & . & . & . & . \\ . & . & . & . & . \\ \triangle X_8 & \triangle Y_8 & \triangle Z_8 & \triangle \Phi_8 & \triangle \Theta_8 \end{bmatrix} \tag{10}$$

Selecting the initial poses of the transmitter coils is important for the "patternsearch" algorithm because according to the manufacturer's instructions,[1] "patternsearch" can find the local minimum. We firstly performed the optimization by choosing initial poses of the transmitter coils within a standard box volume which are similar to the planar field generators of commercial products, as shown in Fig. 4b. For this approach, there are three other preconditions for the optimization. First, the transmitter coils should be placed out of the testing volume. Second, the coils should be positioned at different locations, with a minimum spacing to allow them to be mechanically separated. The calculation of the minimum distance is given by (11).

$$L_{\mathrm{min}} = \sqrt{R_t^2 + \left(\frac{D_t}{2} \right)^2} \tag{11}$$

where R_t is the radius and D_t is the height of the transmitter coils. The third precondition is that the boundaries of the searching vector for the pattern search algorithm should be set within a box volume, i.e., the upper boundary of Z distance is selected to be smaller than 70 mm which is similar to the commercial products. After that, we performed another optimization by removing the boundary limitation into consideration. Therefore, the optimization was performed in a pure 3D volume.

After performing the optimization by searching the maximum of the voltages across the magnetic sensor, we chose the minimum RMSE of the positional accuracy as the optimization target. For this approach, the function to be optimized is given by Eq. (12):

$$F_2 = \sqrt{\frac{\sum_{i=1}^{n} E_{p,i}^2}{n}} \tag{12}$$

Here, $E_{p,i}$ is the sensor position error at each point in the test volume. The optimizations were performed twice similar to searching the maximum voltage. The results have been compared and discussed in the following sections.

Experiment and evaluation

Accuracy according to differences in spatial arrangement of transmitter coils

In this experiment, the transmitters coils were chosen with the material being copper, the radius of 15 mm, the height of 30 mm, and 200 turns of windings. The field generators (FG) of commercial EMTS generally have a small size, e.g. NDI Aurora Planar FG (Northern Digital, Canada) is $200 \times 200 \times 70$ mm in length, width and height respectively. According to this, we defined different poses of the transmitter coils in the simulator to analyze the influences on the tracking accuracy caused by coil arrangement. Figure 4 shows the poses of the transmitter coils and Table 1 shows the detailed spatial arrangement of the coils.

In Fig. 4, the yellow cylinders present the transmitter and sensor coils, respectively. We firstly positioned the transmitter coils within such 3D area with a standard arrangement with all the coil faced toward one orientation, as Fig. 4a shows. After that, in Fig. 4b, each coil was added with multiple 20° and 30° in yaw and pitch angle shift. In Fig. 4e the transmitter coils were located around the VOI with the same orientation, and in Fig. 4f, the transmitter coils were positioned around the VOI with multiple orientations. These

poses of the transmitter coils are stochastically defined. After that, the optimized transmitters' poses were applied.

For each scenario, the tracking accuracy was evaluated. This experiment aims to analyze the influence of the different transmitter coil arrangements on the tracking accuracy.

Testing the performance of the calibration algorithm

In this experiment, we used a standard spatial arrangement of the transmitter coils, i.e., single-plane-multi-orientation, as Fig. 4b illustrates because it is a most conventional planar field generator without optimization. Here, a random shift in position, between −0.5 and 0.5 mm, and in orientation, between −0.5° and 0.5°, are added to each transmitter coils. Table 2 shows the shifts being added to eight transmitter coils. *MATLAB* 'rand' function is used for random number generation. In this evaluation, the generated random shift of the transmitter coils' poses is illustrated in Table 2.

To investigate the robustness of the method, the evaluation of the performance of the calibration was also done using the random shifts as specified Table 2 increased by a factor of 10 and 100, i,e, the deviations were in the range of 0.5, 5 and 50 mm in position shift, and 0.5°, 5° and 50° in the orientation shift. In this evaluation, first, no noise signals were
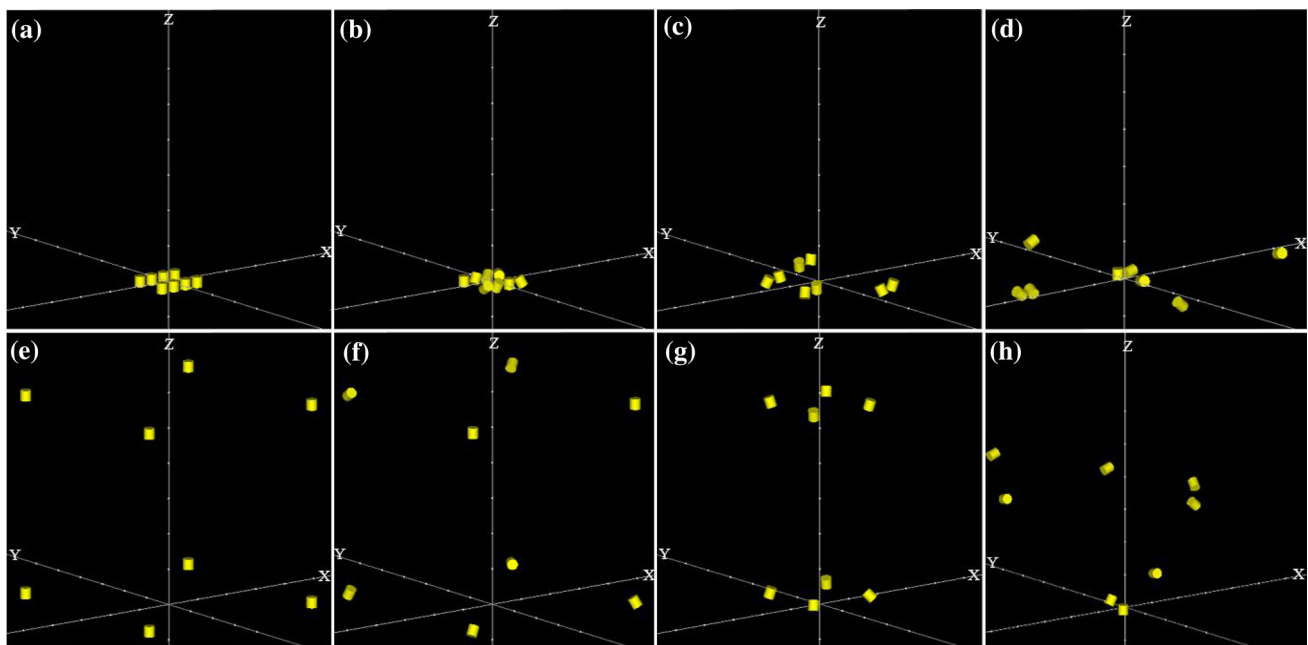

Fig. 4 The stochastically defined position and orientation of the eight transmitter coils: **a** single-plane-single-orientation, the standard transmitter coil arrangement, in one XY plane with one orientation for all the coils, **b** single-plane-multi-orientation, the transmitter coils with multiple orientations in one XY plane, **e** single-orientation and around the volume of interest (VOI), **f** multi-orientation and around VOI. The optimized transmitter coils' pose based on searching for the maximum voltage (**c**) in a box volume and (**g**) in a full 3D space, based on minimizing the sensor position error. And the optimized transmitter coils' pose based on searching for the minimum positional RMSE (**d**) in a box volume and (**h**) in a full 3D space, based on minimizing the sensor position error. The scale along the axis is 100 mm

Table 1 The transmitter coils' arrangement with the IDs from a to h according to Fig. 4

Coil arrangement	Coil no.	1	2	3	4	5	6	7	8
(a,b) Single-plane	X (mm)	−60	−20	20	60	−60	−20	20	60
	Y (mm)	50	50	50	50	−50	−50	−50	−50
	Z (mm)	0	0	0	0	0	0	0	0
(e,f) Around VOI	X (mm)	−300	−300	300	300	−300	−300	300	300
	Y (mm)	−300	−300	300	300	300	300	−300	−300
	Z (mm)	600	0	600	0	600	0	600	0
(a,e) Single-orientation	Φ (°)	0	0	0	0	0	0	0	0
	Θ (°)	0	0	0	0	0	0	0	0
(b,f) Multi-orientation	Φ (°)	0	20	40	60	80	100	120	140
	Θ (°)	0	30	60	90	120	150	180	210
(c) Optimization-maximum voltage (box shape)	X (mm)	74	112.90	−114	−72.90	74	112.90	−114	−72.90
	Y (mm)	184	182.90	−84	−82.90	−184	−182.90	84	82.90
	Z (mm)	0	8.80	0	8.80	0	8.80	0	8.80
	Φ (°)	45	225	45	45	135	315	315	135
	Θ (°)	153.65	162.47	206.35	342.47	206.35	17.53	206.35	197.53
(d) Optimization-minimum RMS error (box shape)	X (mm)	−310	−270	20	60	−60	480	20	60
	Y (mm)	50	50	50	50	−300	−50	−50	450
	Z (mm)	0	0	0	0	0	0	0	0
	Φ (°)	1	257	31	0	6	256.50	251	0
	Θ (°)	125.50	110	0	256	128	255.50	78.25	63.50
(g) Optimization-maximum voltage (around VOI)	X (mm)	97.20	97.20	−97.20	−97.20	97.20	97.20	−97.20	−97.20
	Y (mm)	97.20	97.20	−97.20	−97.20	−97.20	−97.20	97.20	97.20
	Z (mm)	571.20	28.80	571.20	28.80	571.20	28.80	571.20	28.80
	Φ (°)	45	225	45	45	135	315	315	135
	Θ (°)	197.75	197.75	162.25	17.75	162.25	134.25	162.25	162.25
(h) Optimization-minimum RMS error (around VOI)	X (mm)	−280	−280	280	280	−280	−30	−220	280
	Y (mm)	220	−280	30	30	280	30	−280	220
	Z (mm)	330	520	330	270	455	20	80	20
	Φ (°)	258	0	255	0.25	0	1	273	257.50
	Θ (°)	256	251.50	129	132	71	30	0	257.50

Table 2 The added shift to each of the transmitter coils

Coil No.	1	2	3	4	5	6	7	8
$\triangle X$ (mm)	0.1011	0.0369	−0.0492	−0.3852	−0.1208	−0.4132	−0.0382	−0.2443
$\triangle Y$ (mm)	0.2956	−0.1565	−0.4444	0.3971	0.4929	0.3175	0.1244	0.1419
$\triangle Z$ (mm)	−0.2684	0.4684	0.3638	0.3123	−0.1747	−0.0577	0.2663	0.1636
$\triangle\Phi$ (°)	0.0491	0.3687	−0.3103	0.4939	0.3095	−0.2088	0.2121	−0.2074
$\triangle\Theta$ (°)	0.3339	−0.2371	−0.4461	0.0313	−0.3451	−0.3193	−0.1298	−0.0436

added into the measured voltages. Only the influences due to the change in transmitter coils' poses were considered. After that, −100 and −80 dBW noise signals were introduced in the measured voltages to simulate the real-world scenario. The testing volume was the same as defined in evaluation A.

Considering the 50 mm|° measurement error as the worst case, we also performed an experiment to estimate the minimum samples required for the successful calibration process.

In this experiment, we selected between 50 and 726 measured sensor poses to perform the calibration.

Testing the performance of the Kalman filtering

In this experiment, we also selected the transmitter coils' arrangement as Fig. 4b presents. A −100 dBW and AGWN was introduced as well as experiment A. In order to evaluate the dynamic performance of Kalman filter, the sensor coil was

moved in the simulator from $\begin{pmatrix} 0\,\text{mm} \\ 0\,\text{mm} \\ 350\,\text{mm} \end{pmatrix}$ to $\begin{pmatrix} 100\,\text{mm} \\ 200\,\text{mm} \\ 650\,\text{mm} \end{pmatrix}$ at

the velocity of $\begin{pmatrix} 1\,\text{mm/s} \\ 2\,\text{mm/s} \\ 3\,\text{mm/s} \end{pmatrix}$, toward X, Y and Z directions.

The angular velocity of the sensor coil of $\begin{pmatrix} 1°/\text{s} \\ 2°/\text{s} \end{pmatrix}$ starting

from $\begin{pmatrix} -180° \\ -180° \end{pmatrix}$ to $\begin{pmatrix} -80° \\ 20° \end{pmatrix}$. The sensor movement and the pose estimation is synchronized in the simulator by fixing the sampling rate to be 1 Hz. In total, 100 sensor poses were measured in this experiment.

Results

Accuracy according to differences in spatial arrangement of transmitter coils

The changes in the transmitter coils' arrangement also lead to variations in the tracking accuracy. The tracking errors corresponding to different transmitter coils' arrangement were evaluated and shown in Figs. 5 and 6.

As introduced by Figs. 5 and 6, when the coils are facing to one direction, even at lower layers, significant orientation errors exist. Compared to the results for other scenarios, both

position and orientation error are much greater. The tracking accuracy is increased by placing the planar transmitter coils with multiple orientations as (b) and (f) illustrate.

By placing the coils around the VOI, the tracking accuracy is significantly improved compared to placing the coils in a planner area. Multiple orientations of the transmitter coils also benefit from the improvement of tracking accuracy. As (g) and (h) show, after being optimized in a 3D space, the accuracy is further improved. The detailed description of the tracking accuracy is indicated by Table 2. In Figs. 5 and 6, there were no significant differences between both optimization methods.

The performance of the calibration algorithm

The measurement errors of the transmitter coils' positions and orientations were reduced to approximately to 0 for the 3 scenarios. Figure 7 shows the result of cumulative errors of the transmitter coils' positions and orientations after calibration.

As Fig. 7a presents, when there are no noise signals introduced, the calibration algorithm corrects the measurement errors well. The difference is that with larger errors, the calibration algorithm needs more iterations to proceed. After being calibrated, the total errors of the transmitters have all being reduced to a very small value in both position and orientation. As (b), (c), (e) and (f) illustrate, the

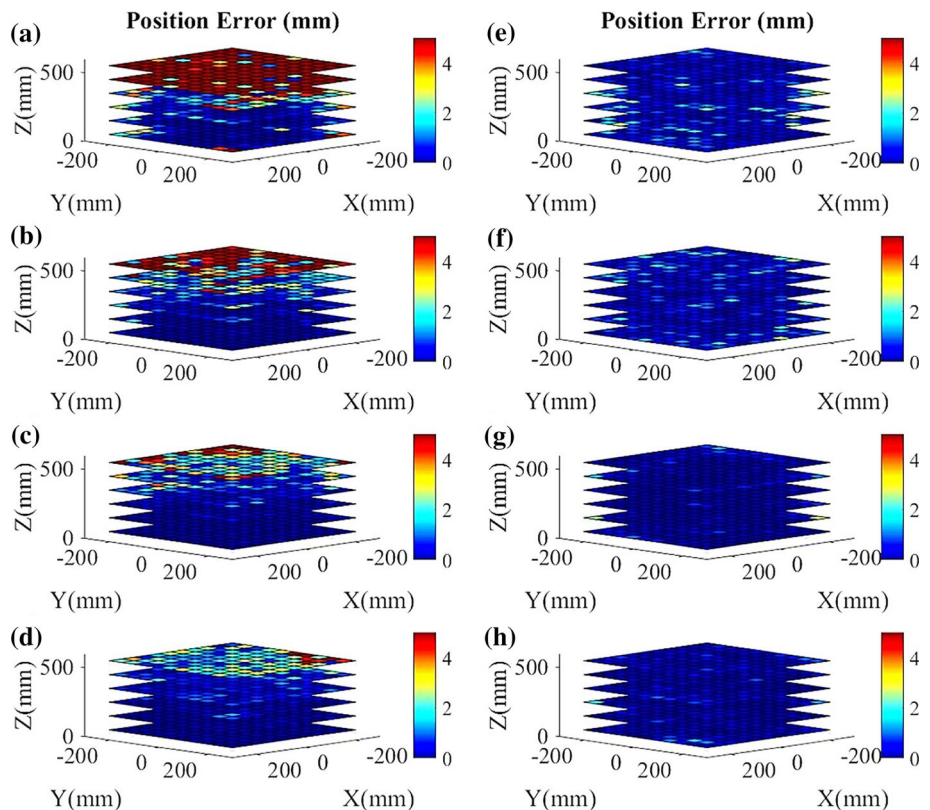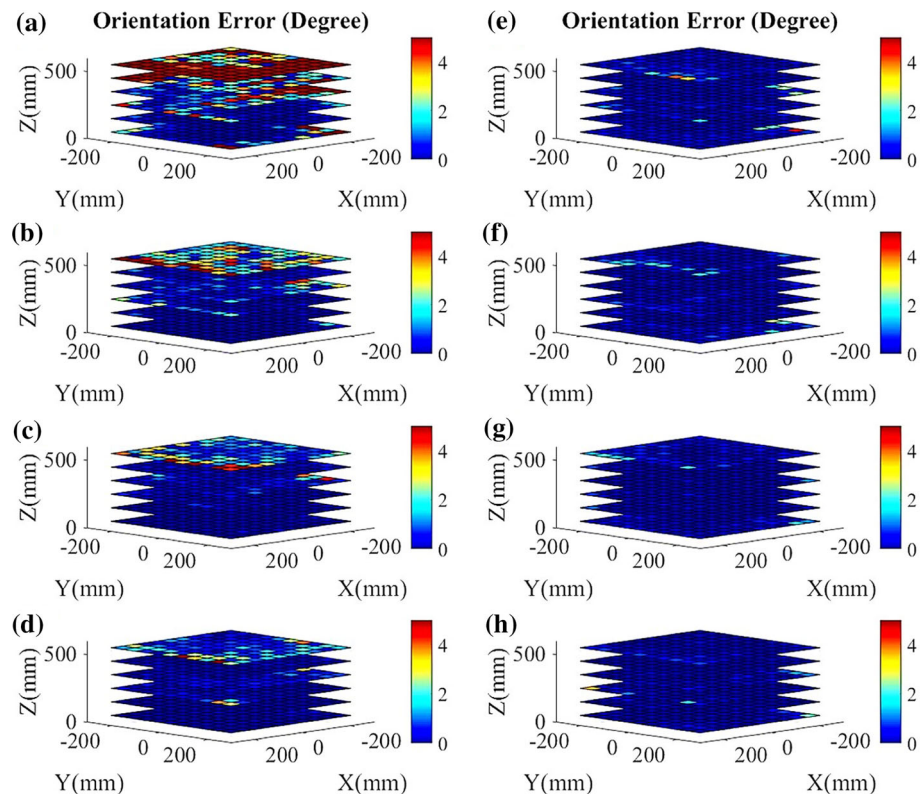Fig. 5 The plot of sensor position error according to coil arrangement introduced in Fig. 4

Fig. 6 The plot of sensor orientation error according to coil arrangement introduced in Fig. 4

Discussion and future work

We present a method of developing a simulator which allows advanced analysis in EMTS. The main drawback of the dipole approximation is it cannot be utilized in the regions too close to the dipole [29]. Therefore, in this work, the VOI for all the experiments was chosen with a minimum Z distance of 50 mm away from the origin XY plane. It is similar to the realities where generally the field generator is placed some distance away from the VOI for surgical applications. The simulator allows the analysis to be conducted in a virtual world where all the unavoidable errors and uncertainties can be removed or separately considered. In this work, the tracking errors caused by the Gaussian white noise in the measured voltages and the inaccuracy in the measured transmitter coils' arrangement were separately analyzed. The noise level was fixed at -100 dBW. It can also be adjusted to simulate the real systems, if the noise level has been previously measured. Another important parameter for simulating the real system is the frequency of the excitation signals. As introduced in "EM Tracking" section, the signal's frequency is proportional to the voltage induced in the sensor coil in a certain bandwidth. Thus, with the same noise level, a higher signal frequency provides a higher SNR.
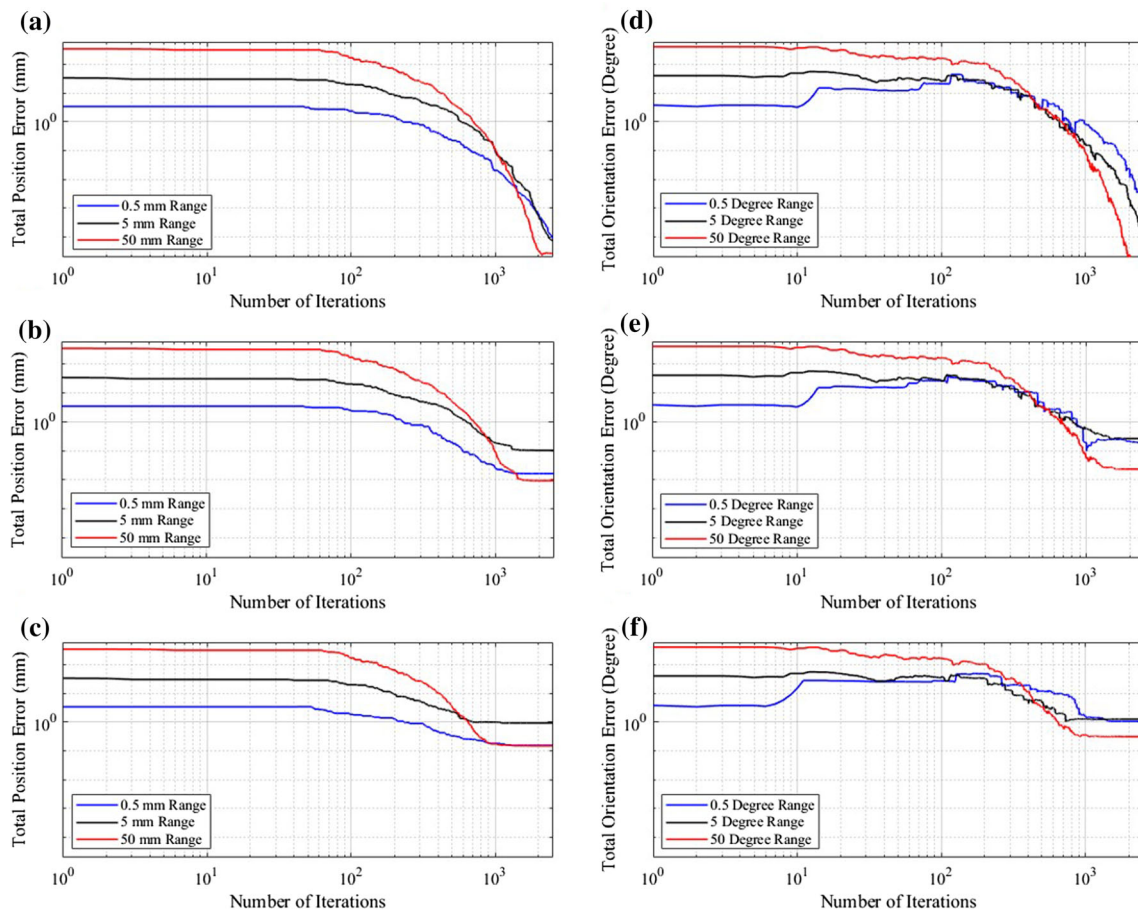
calibration becomes worse in the presence of noises in the measured voltages. This is because—as long as the number of measurements is not infinite,—the noise provides contradictory data and therefore no exact solution in terms of transmitter coils' arrangement exists. Another reason is that the adaptation algorithm may run into local minimum.

As presented in Fig. 8, the calibration algorithm of correcting transmitter coils measurement errors requires a certain amount of sensor locations. When less than 100 points were applied, the calibration algorithm cannot rectify the measurement errors.

Testing the performance of the Kalman filtering

The result of evaluating the dynamic Kalman filter performance with is shown in Fig. 8. The tracking errors increase when the Z distances between sensor and transmitter coils become larger. After applying Kalman filter, the pose errors were reduced to a much lower level.

Figure 9b, c show the improvement in tracking accuracy by employing Kalman filter. The RMS errors before filtering are 5.28 mm and 5.51°, which have been reduced to 0.82 mm and 0.69° after being filtered.

Fig. 7 The change in transmitter coils pose errors during the calibration process: **a**, **d** without noise included, **b**, **e** with −100 dBW and **c**, **f** with −80 dBW Gaussian white noise added in the measured voltages
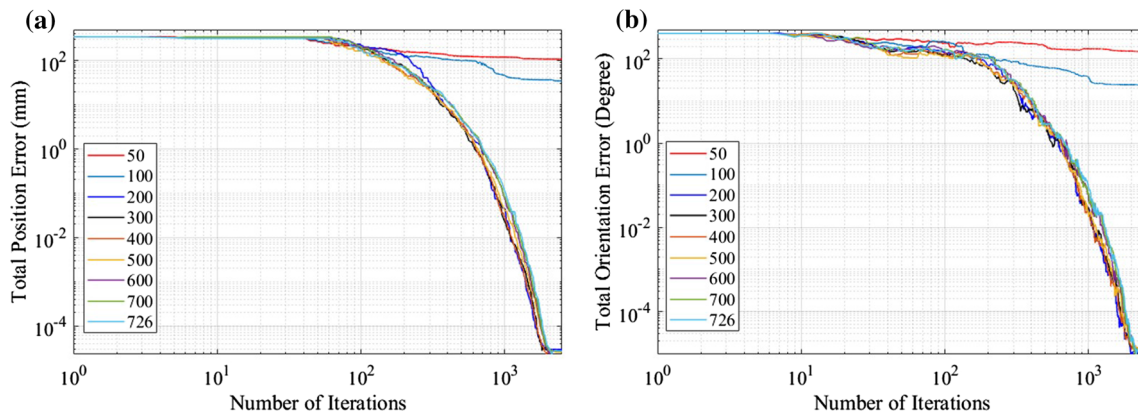

Fig. 8 The transmitter coils' accumulative **a** position errors and **b** orientation errors change during the calibration process with the number of poses for the calibration algorithm being selected between 50 and 726 with the error range of 50 mm|°

In this work, the parameter selection was based on our self-developed experimental setup [10]. The amplitude and frequency of the generated sine-wave signals for the transmitter coils were 1 V and 1 kHz as a standard. In the previous work on the real system, the sensor positional mean error was measured to be 6.9 and 2.15 mm before and after the

calibration. The calibration algorithm cannot further reduce the tracking error because of the existing noises, registration errors, and the tracking errors of the OTS itself, etc. In this work, the sources of errors have been separately analyzed. For a comparison between the simulated result and our experimental setup, we adjusted the parameters in the simulator,
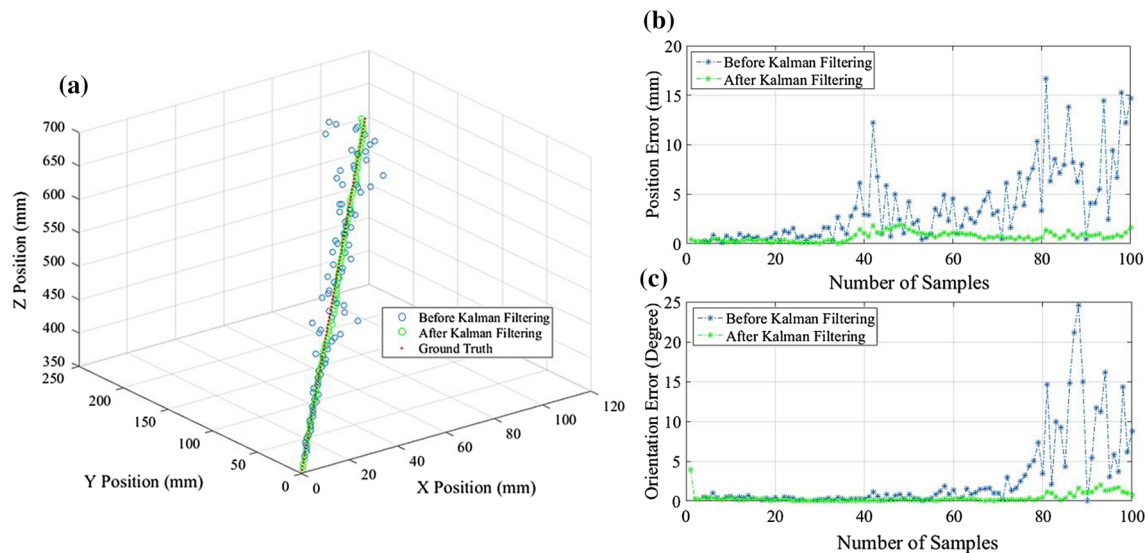
Fig. 9 Evaluation of the dynamic Kalman Filter performance in EM tracking. **a** 3D scatter plot of non-filtered, filtered and ground truth of the sensor positions, **b** and **c** present the sensor's position and orientation errors being reduced after applying Kalman Filter

to let them exactly match our system by changing the poses, radius, and turns of the coils. The testing volume was also redefined to be 240 mm × 240 mm × 180 mm, which is the same as the testing volume for our EMTS prototype. When only considering the noise, the mean positional error was 0.16 mm; when only considering the shift in the transmitter coils' arrangement, the mean positional error was evaluated to be 5.24 mm. After being calibrated, the tracking error was reduced to be less than 0.01 mm without considering the noise and other uncertainties. The simulator can also be applied to allow a comprehensive comparison between the simulation and any other real systems and performing tests without always requiring the hardware.

The developed simulator provides a framework for simulating the entire EMTS. It also allows other sources of errors, such as the conductive distortions caused by metallic materials in medical instruments and devices in operating rooms, to be implemented for more advanced analysis in the future. However, the implementation of ferromagnetic distortions could be more challenging, because of the nonlinearity of the magnetic susceptibility of ferromagnetic materials [30].

To assess the tracking accuracy, in this work, a standard testing volume of $500 \times 500 \times 500\ mm^3$ was chosen. The testing volume and sensor pose can be customized within the simulator, allowing the simulations of real tracking applications.

This work focuses on the analysis of a typical 5-DOF medical EMTS in assisting IGS. Most commercial EMTS utilize a planar field generator [4]. For a typical 5-DOF EMTS, at least five transmitter coils are required for "solving" the 5-DOF parameters. The additional coils provide more comprehen-

sive information for the optimization algorithm. For the real systems, eight transmitter coils are commonly applied [20,21,30]. Therefore, this number was also chosen in this work to let the simulator be adaptable for other setups and enable customization. For comparison, we firstly compared the tracking accuracy with all the transmitter coils placed in a planar field generator. The result shows that when the coils are faced in a single orientation, the system has the worst accuracy. Accuracy is improved by applying multiple coil orientations and further enhanced by the optimized transmitter coil arrangement to get the largest voltages across the sensor coil. Placing the transmitter coils around the VOI improved the tracking accuracy to a high level. The optimization of the coil arrangement further improved the tracking accuracy.

The comparison between using the different objective functions for the optimization algorithm is presented in Table 3. The results illustrate that choosing the sensor position RMSE as the objective function let the system have an even better accuracy. In the box-area, the both optimized coil arrangement can be easily applied in reality. However, as shown in Fig. 4h, the optimized transmitter coils are not symmetric to each other in a 3D VOI, which may add complexities in the construction process. In this work, the objective functions were defined to either maximize the induced mean voltages or minimize the positional RMSE of the sensor coil within the defined testing volume. In the future, more parameters can also be selected for the optimizations. For example, in some applications where orientations errors need to be focused, a more advanced objective function also considering the sensor orientation errors needs to be defined.

Table 3 The tracking errors of the 726 sensor poses due to different spatial arrangement of the transmitter coils

Coil arrangement	a	b	c	d	e	f	g	h
Position error (mm)								
Mean	7.98	1.67	0.84	0.61	0.57	0.52	0.24	0.22
RMS	17.02	3.41	1.60	1.15	0.80	0.72	0.48	0.31
Max	128.91	31.11	10.16	11.21	6.45	6.73	3.86	1.72
95th	36.19	6.75	3.50	2.59	1.58	1.43	0.97	0.65
Orientation error (°)								
Mean	6.49	1.60	0.84	0.50	0.46	0.38	0.32	0.26
RMS	19.07	6.29	5.19	1.84	1.61	1.27	1.16	1.03
Max	265.42	78.89	118.68	32.3	28.69	16.61	20.32	17.56
95th Percentile	28.18	4.62	2.82	1.78	1.52	1.16	0.97	0.80

The calibration algorithm for correction of the measurement errors of the transmitter coils' poses was evaluated by using the simulator without considering noises, errors of the reference positioning system and other uncertainties from the real world. The results show that the algorithm itself works correctly without noises. When noises were introduced in the voltage measurement, the calibration algorithm cannot perfectly correct measurement errors in the transmitter coils' pose. The performance of Kalman filtering has also been tested based on the simulator. The result shows that applying Kalman filter is promising to enlarge the actual working volume. However, the Kalman filter solely reduces the sensor jitter errors caused by the noises. The actual tracking accuracy (correctness) cannot be improved by applying Kalman filter. In the future work, more complex noise models can be selected to perform a systematic analysis to evaluate the performance of Kalman filter in EM tracking.

The proposed simulator can also be applied to analyze other system parameters and testing new applications in electromagnetic tracking, before trying them on a real system setup. It removes the uncertainties from the reality and can be applied to speeding up developing new technologies. In addition, the simulator can also be adapted to 6-DOF tracking system by adding an additional sensor coil with a fixed pose to the first sensor coil [31]. It will allow the rotation angle to be estimated.

Conclusion

Various sources of errors influence the accuracy of electromagnetic tracking systems. A real-world system does not allow the sources of errors to be analyzed individually. Therefore, we developed software to simulate the entire electromagnetic tracking system. The ground truths of the sensor coils' position and orientation can always be known within the simulator. System parameters such as noise level and transmitter coil poses can also be separately adjusted in the simulator. In this work, the optimization of the transmitter coil arrangement and the comparisons of tracking accuracy according to different transmitter coil poses were performed. The results show that the EMTS is more accurate when the transmitter coils are placed around the VOI in an optimized layout. The results also indicate that the calibration algorithm can correct the measurement errors of the transmitter coils' poses. The Kalman filter is promising to enlarge the working volume of electromagnetic tracking systems. The developed simulator also supports other analysis in general EM tracking.

References

1. Loke WF, Choi TY, Maleki T, Papiez L, Ziaie B, Jung B (2010) Magnetic tracking system for radiation therapy. IEEE Trans Biomed Circuits Syst 4(4):223–231. doi:10.1109/TBCAS.2010.2046737
2. Franz AM, März K, Hummel J, Birkfellner W, Bendl R, Delorme S, Schlemmer HP, Meinzer HP, Maier-Hein L (2012) Electromagnetic tracking for us-guided interventions: standardized assessment of a new compact field generator. Int J Comput Assist Radiol Surg 7(6):813–818. doi:10.1007/s11548-012-0740-3
3. Shahriari N, Hekman E, Oudkerk M, Misra S (2015) Design and evaluation of a computed tomography (ct)-compatible needle insertion device using an electromagnetic tracking system and ct images. Int J Comput Assist Radiol Surg 10(11):1845–1852. doi:10.1007/s11548-015-1176-3
4. Franz AM, Haidegger T, Birkfellner W, Cleary K, Peters TM, Maier-Hein L (2014) Electromagnetic tracking in medicine—a review of technology, validation, and applications. IEEE Trans Med Imaging 33(8):1702–1725. doi:10.1109/TMI.2014.2321777

5. Wood BJ, Zhang H, Durrani A, Glossop N, Ranjan S, Lindisch D, Levy E, Banovac F, Borgert J, Krueger S, Kruecker J, Viswanathan A, Cleary K (2005) Navigation with electromagnetic tracking for interventional radiology procedures: a feasibility study. J Vasc Interv Radiol 16(4):493–505. doi:10.1097/01.RVI.0000148827.62296.B4

6. Krücker J, Xu S, Glossop N, Viswanathan A, Borgert J, Schulz H, Wood BJ (2007) Electromagnetic tracking for thermal ablation and biopsy guidance: clinical evaluation of spatial accuracy. J Vasc Interv Radiol 18(9):1141–1150. doi:10.1016/j.jvir.2007.06.014

7. Yaniv Z, Wilson E, Lindisch D, Cleary K (2009) Electromagnetic tracking in the clinical environment. Med Phys 36(3):876–892. doi:10.1118/1.3075829

8. Hummel J, Figl M, Birkfellner W, Bax MR, Shahidi R, Maurer C Jr, Bergmann H (2006) Evaluation of a new electromagnetic tracking system using a standardized assessment protocol. Phys Med Biol 51(10):N205. doi:10.1088/0031-9155/51/10/N01

9. Bien T, Li M, Salah Z, Rose G (2014) Electromagnetic tracking system with reduced distortion using quadratic excitation. Int J Comput Assist Radiol Surg 9(2):323–332. doi:10.1007/s11548-013-0925-4

10. Bien T, Rose G (2012) Algorithm for calibration of the electromagnetic tracking system. In: 2012 IEEE-EMBS international conference on biomedical and health informatics (BHI), IEEE, pp 85–88. doi:10.1109/BHI.2012.6211512

11. Fitzpatrick JM, West JB, Maurer CR (1998) Predicting error in rigid-body point-based registration. IEEE Trans Med Imaging 17(5):694–702. doi:10.1109/42.736021

12. Frantz DD, Wiles A, Leis S, Kirsch S (2003) Accuracy assessment protocols for electromagnetic tracking systems. Phys Med Biol 48(14):2241

13. Nafis C, Jensen V, Beauregard L, Anderson P (2006) Method for estimating dynamic em tracking accuracy of surgical navigation tools. Proc SPIE Med Image 2006 Vis Image Guided Proc Display 6141:152–167. doi:10.1117/12.653448

14. Wilson E, Yaniv Z, Zhang H, Nafis C, Shen E, Shechter G, Wiles A, Peters T, Lindisch D, Cleary K (2007) A hardware and software protocol for the evaluation of electromagnetic tracker accuracy in the clinical environment: a multi-center study. Proc SPIE 6509:65092T. doi:10.1117/12.712701

15. Koivukangas T, Katisko JP, Koivukangas JP (2013) Technical accuracy of optical and the electromagnetic tracking systems. SpringerPlus 2(1):90. doi:10.1186/2193-1801-2-90

16. O'Donoghue K, Cantillon-Murphy P (2015) Planar magnetic shielding for use with electromagnetic tracking systems. IEEE Trans Magn 51(2):1–12. doi:10.1109/TMAG.2014.2352344

17. Li M, Hansen C, Rose G (2015) A robust electromagnetic tracking system for clinical applications. In: Proceedings of the annual meeting of the German society of computer- and robot-assisted surgery, pp 31–36

18. Wiles AD, Thompson DG, Frantz DD (2004) Accuracy assessment and interpretation for optical tracking systems. Proc SPIE 5367:421–432. doi:10.1117/12.536128

19. Maier-Hein L, Franz A, Birkfellner W, Hummel J, Gergel I, Wegner I, Meinzer HP (2012) Standardized assessment of new electromagnetic field generators in an interventional radiology setting. Med Phys 39(6):3424–3434

20. Plotkin A, Shafrir O, Paperno E, Kaplan DM (2010) Magnetic eye tracking: a new approach employing a planar transmitter. IEEE Trans Biomed Eng 57(5):1209–1215. doi:10.1109/TBME.2009.2038495

21. O'Donoghue K, Eustace D, Griffiths J, O'Shea M, Power T, Mansfield H, Cantillon-Murphy P (2014) Catheter position tracking system using planar magnetics and closed loop current control. IEEE Trans Magn 50(7):1–9. doi:10.1109/TMAG.2014.2304271

22. Raab FH, Blood EB, Steiner TO, Jones HR (1979) Magnetic position and orientation tracking system. IEEE Trans Aerosp Electron Syst AES 15(5):709–718. doi:10.1109/TAES.1979.308860

23. Schneider M, Stevens C (2007) Development and testing of a new magnetic-tracking device for image guidance. In: Medical imaging, International society for optics and photonics, pp 65.090I–65.090I. doi:10.1117/12.713249

24. Sherman JT, Lubkert JK, Popovic RS, DiSilvestro MR (2007) Characterization of a novel magnetic tracking system. IEEE Trans Magn 43(6):2725–2727. doi:10.1109/TMAG.2007.893314

25. Stenger B, Mendonça PR, Cipolla R (2001) Model-based hand tracking using an unscented Kalman filter. BMVC 1:63–72. doi:10.5244/C.15.8

26. Bertozzi M, Broggi A, Fascioli A, Tibaldi A, Chapuis R, Chausse F (2004) Pedestrian localization and tracking system with Kalman filtering. In: Intelligent vehicles symposium, IEEE, pp 584–589. doi:10.1109/IVS.2004.1336449

27. Schenderlein M, Rasche V, Dietmayer K (2011) Three-dimensional catheter tip tracking from asynchronous biplane X-ray image sequences using non-linear state filtering. In: Bildverarbeitung für die Medizin 2011, Springer, pp 234–238. doi:10.1007/978-3-642-19335-4_49

28. Li M, Song S, Hu C, Chen D, Meng MQH (2010) A novel method of 6-dof electromagnetic navigation system for surgical robot. In: 2010 8th world congress on intelligent control and automation (WCICA), IEEE, pp 2163–2167. doi:10.1109/WCICA.2010.5554348

29. Harris PG, Pendlebury J (2006) Dipole-field contributions to geometric-phase-induced false electric-dipole-moment signals for particles in traps. Phys Rev A 73(1):014101. doi:10.1103/PhysRevA.73.01410

30. Li M, Hansen C, Rose G (2017) A software solution to dynamically reduce metallic distortions of electromagnetic tracking systems for image-guided surgery. Int J Comput Assist Radiol Surg 2:1–13. doi:10.1007/s11548-017-1546-0

31. Aron M, Kerrien E, Berger MO, Laprie Y (2006) Coupling electromagnetic sensors and ultrasound images for tongue tracking: acquisition setup and preliminary results. In: 7th international seminar on speech production-ISSP'06, CEFALA-Centro de Estudos da Fala, Acústica, Linguagem e músicA